PROCEEDINGS OF SCIENCE

Study of forward particle production in $\sqrt{s}$ = 13 TeV proton-proton collisions with ATLAS-LHCf detectors

Qi-Dong Zhou[*a] **for the LHCf Collaboration**

[a] *Institute for Space-Earth Environmental Research, Nagoya University, Nagoya, Japan*

E-mail: zhouqidong@isee.nagoya-u.ac.jp

Collider experiment is an efficient way to verify and improve the hadronic interaction models. Abundant of energy flow in the forward region of the collisions are believed to have large influence to the development of air-shower. LHCf is the experiment dedicate to verify the hadronic interaction models by measuring the forward neutral particle production at the LHC. According to the LHCf results, no simulation model can predict the LHCf data perfectly. Thus, it is necessary to classify the LHCf observables into specific interaction types; diffraction and non-diffraction. Several Monte Carlo simulation samples in p-p collisions at $\sqrt{s}$ = 13 TeV were analyzed for studying the presence of differences among specific interaction types on the LHCf observables. Combining the information of ATLAS, LHCf can identify these specific interaction types experimentally, especially, the low mass diffraction. LHCf and ATLAS have succeed the common data-taking in p-p collisions at $\sqrt{s}$ = 13 TeV. The recent joint analysis result will be reported.

35th International Cosmic Ray Conference
10-20 July, 2017
Bexco, Busan, Korea

*Speaker.

PoS(ICRC2017)215

1. Introduction

The properties of primary high energy Cosmic-Rays (CRs) are usually reconstructed from the measured characteristics of so-called extensive air showers. The determination of composition and energy of CRs depend strongly on the Monte Carlo (MC) simulations of air showers at high energies. Such MC simulations are made by assuming the hadronic interactions which are hardly predicted theoretically, especially, the soft processes. The limitation in the modeling of hadronic interactions and the largely unknown model uncertainties lead to the large uncertainties in interpreting the measurement data [1, 2].

The inelastic hadronic collisions are usually classified into *soft processes* and *hard processes*. Most parts of the hard processes can be treated within the theoretical framework, based on the perturbative quantum chromodynamics (QCD) owing to the large momentum transfer. However, it is inadequate to describe the soft processes such as diffractive dissociations. Instead, a phenomenology of soft hadronic processes was employed to describe these processes at high energies, based on the Gribov-Regge theory [3, 4]. Therefore, it is extremely important to constrain the phenomenological parameters based on the measurement data for correct understanding of soft processes and their accurate contribution. The LHC forward (LHCf) experiment [5] is capable of measuring the neutral particle productions at ZERO degree of LHC, which are believed to play an important role in the development of air showers. The expriment allows to provide unique measurement data of soft processes at 10^{17} eV as the laboratory equivalent collision energy. In particular, LHCf had a common data acquisition with ATLAS in $\sqrt{s}$ = 13 TeV operation. The ATLAS central information makes it possible to identify the type of the LHCf observed collisions at event by event bias; diffraction and non-diffraction. Consequently, the ATLAS-LHCf common operation is able to provide more specific experiment data for constraining hadronic interaction models.

In the present work, three subjects were investigated based on MC simulation. We first investigated the different contributions of non-diffractive and diffractive components to the forward neutral particle cross sections and the differences among models. Then, we evaluated the performance to identify the diffractive dissociation on the corresponding cross sections of neutral particles expected by the LHCf detector by applying a simple selection based on ATLAS central information. Finally, we studied the sensitivity range in diffractive mass of the common experiment using LHCf and ATLAS detectors.

2. Diffractive dissociation

In high energy proton-proton interactions, the Regge theory describes diffractive processes as the t-channel reactions, which is dominated by the exchange of an object with vacuum quantum numbers so called *Pomeron* [6, 7]. As shown in Fig.1, there is an operational characteristic of diffractive interactions, which is a large angle separation between the final state systems of X and P_3 so called rapidity gap $\Delta\eta$. The $\Delta\eta$ size and the location of them in the pseudorapidity phase-space can be used to determine the type of the diffractions. It has been known that the relationship between the observable $\Delta\eta$ size and ξ_X is $\Delta\eta \simeq -\ln(\xi_X)$, where $\xi_X = M_X^2/s$, M_X is diffractive mass (invariant mass of dissociated system of proton). It is known that the $\Delta\eta$ size and inelasticity has relationship as $K_{inel} \simeq \exp(-\Delta\eta)$.

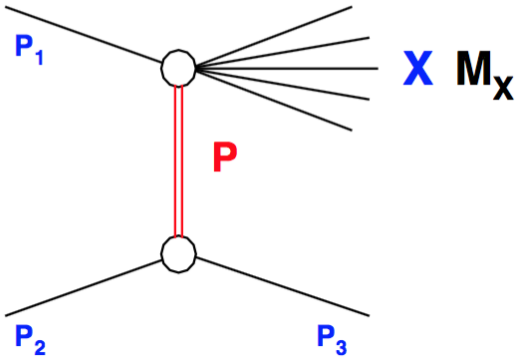

Figure 1: The figure illustrates the single-diffraction with the pomeron exchanged in a proton-proton collision. M_X is the invariant masses of the dissociated systems X.

3. Diffractive and non-diffractive contributions to the LHCf photon spectra

As shown in Fig. 2, When ATLAS [14] and LHCf [5] observe the same collision, LHCf covers the very forward region and ATLAS has sensitivities to the central region. The ATLAS inner detector (ID) measures particle momentum and vertex information with full azimuthal (ϕ) and $|\eta| <$ 2.5 pseudorapidity coverage. For studies of minimum-bias measurements, this detector can provide information on charged tracks with a p_T threshold as low as 100 MeV. The LHCf detectors were installed in the target neutral absorber (TAN) located $\pm$140 m from IP1. The detectors were designed to measure forward neutral particles (e.g., neutrons, photons, and π^0s) over a pseudorapidity range $|\eta| > 8.4$. The photon and hadron energy thresholds are 200 and 500 GeV, respectively. Therefore, LHCf can classify the measured events according to the rapidity gap of the final state measured by ATLAS.

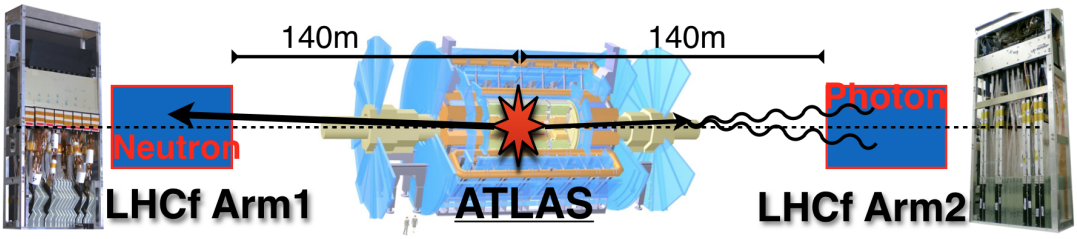

Figure 2: The LHCf detectors and their location.

In this analysis, the MC simulations were produced using four interaction models; EPOS-LHC [8], QGSJET-II-04 [9], SYBILL 2.3 [10, 11], and PYTHIA 8212 [12, 13]. Each event sample is classified into non-diffractive and diffractive collisions by using MC flags. The simulated photon spectra are shown in the right pads of Fig. 3 for a fiducial area of the LHCf analyses, $|\eta| >$10.94. Clearly, the non-diffraction and diffraction implemented in each model are very different, especially, the diffractive contribution of PYTHIA8212 has a big excess at the large energies. This leads to the big discrepancy between PYTHIA8212 and data, which are shown in the left pad of Fig. 3.

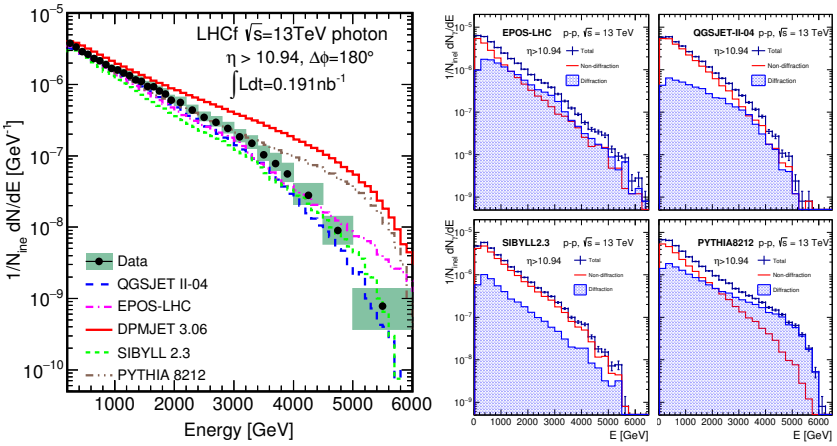

Figure 3: The LHCf photon spectra in pp collisions at $\sqrt{s}$ = 13 TeV. The photon spectrum at $\eta > 10.94$ are shown by comparing with hadronic interaction models. The diffractive contribution of EPOS-LHC, QGSJET-II-04, SYBILL 2.3 and PYTHIA 8212 are shown.

4. Identification of diffraction with ATLAS track information

Because of the large differences found among different hadronic interaction models, it is important to classify the observed LHCf spectra into non-diffraction or diffraction experimentally. The method of diffraction and non-diffraction identification by using ATLAS information and the corresponding performance were investigated by using MC simulation.

4.1 Criteria of diffraction selection

Table 1: The efficiency and purity of diffraction selection with different ATLAS veto selection conditions.

Treatments	N_{track}**=0**	$N_{track} \leq$**1**	$N_{track} \leq$**2**	$N_{track} \leq$**5**
Efficiency(ε)	0.493	0.556	0.619	0.691
Purity(p)	0.995	0.991	0.982	0.950

The identification of diffraction requires large rapidity gap, consequently small number of particles is expected in the central detector, for instance, the ATLAS detector. Basic idea in this analysis is if an event has a small N_{track} (the number of charged particles with $P_T > 100$ MeV at $|\eta| < 2.5$), it is more likely a diffractive event. In the other words, existence of charged tracks in the ATLAS rapidity range is used to veto non-diffrative events. It is assumed that the ATLAS detector can count the number of charged particle tracks, N_{track}. Performance of ATLAS-veto event selection were studied for different criteria as listed in Table 1. According to MC true flags, events can be classified as non-diffraction (ND), central diffraction (CD), single diffraction (SD) and double diffraction (DD). By applying the ATLAS-veto selection to each event, the selection efficiency (ε) and purity (p) of diffractive event selection are defined as

$$\varepsilon = \frac{(N_{CD}+N_{SD}+N_{DD})_{ATLAS\ veto}}{N_{CD}+N_{SD}+N_{DD}} \tag{4.1}$$

$$p = \frac{(N_{CD}+N_{SD}+N_{DD})_{ATLAS\ veto}}{(N_{ND}+N_{CD}+N_{SD}+N_{DD})_{ATLAS\ veto}}. \tag{4.2}$$

where $N_{ND,CD,SD,DD}$ means number of event in each event category. The suffix $_{ATLAS\ veto}$ means number of event after applying the ATLAS-veto event selection. Consequently,

- *no charged particle (N_{track}=0) in the kinematic range $|\eta|$ <2.5 and p_T >100 MeV,*

is adopted as ATLAS-veto selection condition.

4.2 The performance of ATLAS-veto selection

To evaluate the performance of the ATLAS-veto selection, the LHCf spectra were classified to non-diffractive-like and diffractive-like according to ATLAS-veto selection. The accurate performances of the selection were evaluated by adapting the Eq.4.1 and Eq.4.2 to the LHCf photon spectrum. As shown in Figs.4 and Figs.5, it is clear that selection purity stays constantly high (at $\approx$ 100%), independent of particle type, energy, and MC simulation model, whereas selection efficiency has a tendency to increase with increasing energy. In contrast to selection purity, selection efficiency exhibits differences among MC simulation models. The more detail information was shown in [15].

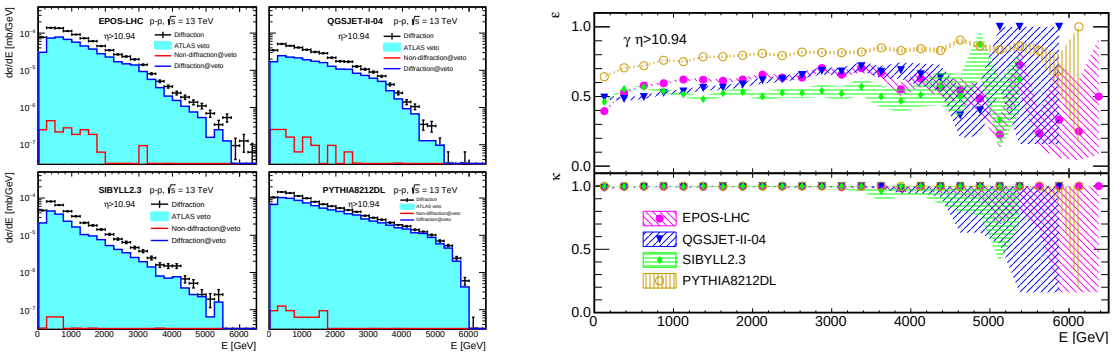

Figure 4: The left figure shows photon spectra at $\eta > 10.94$ generated by EPOS-LHC, QGSJET-I I-04, SYBILL 2.3, and PYTHIA 8212DL. The top four panels show the spectra of true diffraction (black points) and diffractive-like events corresponding to ATLAS-veto selection (filled gray areas), in addition, the ATLAS-veto events were classified by non-diffraction (red) and diffraction (blue) again according to MC true information. The right figure shows the efficiency and purity of diffraction selection by using ATLAS-veto technique correspond to up and down pads on the figure of right side.

4.3 Low-mass diffraction

The central detectors, for instance ATLAS, have limited acceptance. It limits the measurement of rapidity gap signatures at around $-6 < \log_{10}(\xi_x) < -2$; these correspond to the lower and upper limits of M_X of $\sim$13 and 1300 GeV at $\sqrt{s} = 13$ TeV, respectively. For obtaining the overall inelastic cross section, the central detectors estimated the cross section of low-mass diffractive dissociation by using extrapolation based on MC simulations. On the other hand, the cross section of low-mass diffraction ($M_X < 3.4$ GeV) reported by the TOTEM collaboration by using the Roman Pot technique (indirectly measurement of low mass diffraction) [16], 2.62 ± 2.17 mb [17], at $\sqrt{s} = 7$ TeV. The direct measurement of low mass diffraction is still an open question. The LHCf detectors covering zero-degree collision angles, have unique sensitivity to low mass diffractive processes.

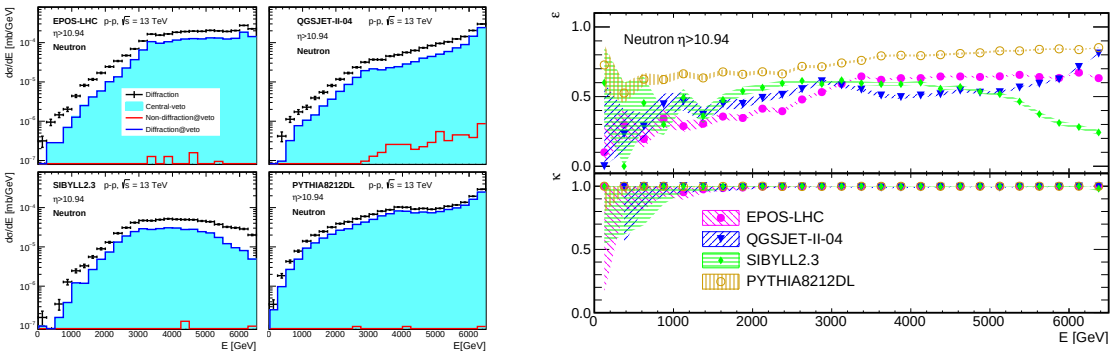

Figure 5: The left figure shows neutron spectra at $\eta > 10.94$ generated by EPOS-LHC, QGSJET-I I-04, SYBILL 2.3, and PYTHIA 8212DL. The top four panels show the spectra of true diffraction (black points) and diffractive-like events corresponding to ATLAS-veto selection (filled gray areas), in addition, the ATLAS-veto events were classified by non-diffraction (red) and diffraction (blue) again according to MC true information. The right figure shows the efficiency and purity of diffraction selection by using ATLAS-veto technique correspond to up and down pads on the figure of right side.

According to QGSJET-II-04 simulation predictions, most of the LHCf detected events survived from the ATLAS-veto selection are from the low-mass diffraction as shown in Fig.6. In particular, all the LHCf detected low-mass diffractive events at $\log_{10}(\xi_x) <$ -5.5 survived from the ATLAS-veto selection. whereas all the high-mass diffractive events at $\log_{10}(\xi_x) > -4$ were excluded. In the other word, the filled histogram in left pad of Figs. 4 and Figs. 5 are mostly derived from the low-mass diffractive processes at $\log_{10}(\xi_x) < -5.5$. Therefore, the LHCf detector combine with ATLAS detector can give a constraint to the treatment of low-mass diffraction implemented in the MC simulation models.

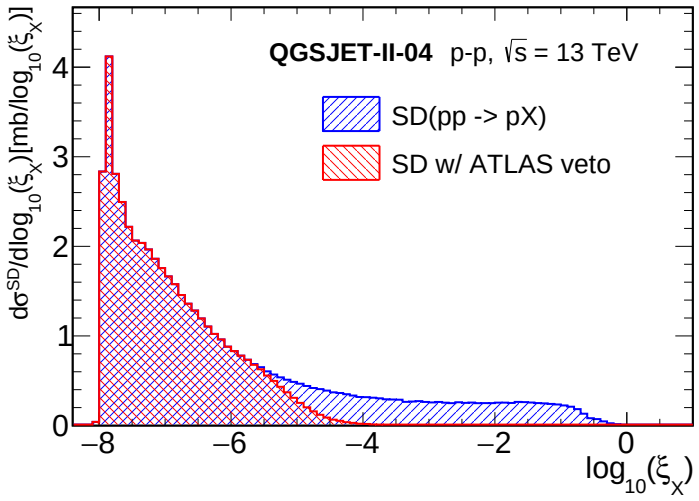

Figure 6: The SD ($pp \to pX$; blue) cross section as a function of $\log_{10}\xi_X$ predicted by using QGSJET-II-04 MC samples. Which is compared with the SD cross section after applying the ATLAS-veto selection (red).

5. Conclusions

We studied the non-diffractive and diffractive contributions to the LHCf spectra using MC predictions in p–p collisions at $\sqrt{s} = 13$ TeV. Non-diffraction and diffraction have different contribution in the very forward regions, the predictions of hadronic interaction models also exhibit big discrepancies among each other. The rapidity gap measurement (central-veto technique) using ATLAS information is an effective way to identify diffractive events and classify the forward productions to non-diffraction and diffraction. Furthermore, the ATLAS-LHCf common operation is capable of both constraining the differential cross sections ($d\sigma/dE$, $d\sigma/d\eta$) of low-mass diffraction and helping to identify the inherent problems in the models corresponding to low-mass diffraction.

References

[1] R. Ulrich, R. Engel, and M. Unger, Phys. Rev. D **83**, 054026 (2011)

[2] K.-H. Kampert and M. Unger, Astropart. Phys. **35**, 660–678 (2012)

[3] V. Gribov, Sov. Phys. JETP **30**, 414 (1968).

[4] T. Regge, Nuovo, Ciment **14**, 951–976 (1959).

[5] LHCf Collaboration, JINST, **3**, S08006 (2008)

[6] E. Feinberg, I. Pomerancuk, Suppl. Nuovo Cim. **3**, 652 (1956).

[7] G. Chew and S. Frautschi, Phys. Lett. **7**, 394 (1961)

[8] T. Pierog et al., Phys. Rev. C **92**, 034906 (2015)

[9] S. Ostapchenko, Phys. Rev. D **83**, 014018 (2011)

[10] E.-J. Ahn, R. Engel, T. K. Gaisser, P. Lipari, and T. Stanev, Phys. Rev. D **80**, 094003 (2009)

[11] R. Engel, T. K. Gaisser, F. Riehn, and T. Stanev, Proc. 34th Int. Cosmic Ray Conf., The Hague (The Netherlands), 1313 (2015)

[12] T. Sjöstrand, S. Mrenna, and P. Skands, JHEP **05**, 026 (2006)

[13] T. Sjöstrand, S. Mrenna, and P. Skands, Comput. Phys. Commun. **178**, 852 (2008)

[14] ATLAS Collaboration, JINST, **3**, S08003 (2008)

[15] Qi-Dong Zhou et al. Eur. Phys. J. C **77** 212 (2017)

[16] TOTEM Collaboration, JINST, **3**, S08007 (2008)

[17] TOTEM Collaboration (G. Antchev et al.), Europhys. Lett. **101**, 21003 (2013)

PoS(ICRC2017)215